THE ASTROPHYSICAL JOURNAL, 318:161–174, 1987 July 1


# A STUDY OF A FLUX-LIMITED SAMPLE OF *IRAS* GALAXIES[1]

BEVERLY J. SMITH AND S. G. KLEINMANN
University of Massachusetts
J. P. HUCHRA
Harvard-Smithsonian Center for Astrophysics
AND
F. J. LOW
Steward Observatory, University of Arizona
*Received 1986 September 3; accepted 1986 December 11*

## ABSTRACT

We present results from a study of all 72 galaxies detected by *IRAS* in band 3 at flux levels $\geq 2$ Jy and lying the region $8^h < \alpha < 17^h$, $23^\circ.5 < \delta < 32^\circ.5$. Redshifts and accurate four-color *IRAS* photometry were obtained for the entire sample. The 60 $\mu$m luminosities of these galaxies lie in the range $4 \times 10^8 (H_0/100)^2\ L_\odot$ to $5 \times 10^{11} (H_0/100)^2\ L_\odot$. The 60 $\mu$m luminosity function at the high-luminosity end is proportional to $L^{-2}$; below $L = 10^{10}\ L_\odot$ the luminosity function flattens. This is in agreement with previous results. We find a distinction between the morphology and infrared colors of the most luminous and the least luminous galaxies, leading to the suggestion that the observed luminosity function is produced by two different classes of objects.

Comparisons between the selected *IRAS* galaxies and an optically complete sample taken from the CfA redshift survey show that they are more narrowly distributed in blue luminosity than those optically selected, in the sense that the *IRAS* sample includes few galaxies of low absolute blue luminosity. We also find that the space distribution of the two samples differ: the density enhancement of *IRAS* galaxies is only $\sim\frac{1}{3}$ that of the optically selected galaxies in the core of the Coma Cluster, raising the question whether source counts of *IRAS* galaxies can be used to deduce the mass distribution in the universe. The percentage of active galaxies is similar in both samples, suggesting that nuclear activity is not a strong contributor to the infrared flux in this sample.

*Subject headings:* galaxies: photometry — infrared: sources

## I. INTRODUCTION

The *IRAS* survey offers the first opportunity to study complete samples of galaxies selected at far-infrared wavelengths. The survey is insensitive to obscuration by dust, though emission from dusty interstellar and circumstellar clouds in the Milky Way causes confusion near the galactic plane (Rowan-Robinson *et al.* 1984). To interpret the source counts in terms of evolution of the space distribution of IR-bright galaxies, it is necessary to know the infrared luminosity function of galaxies, and whether different classes of galaxies contribute to the luminosity function at its high- and low-luminosity extremes. Such a subdivision of the luminosity function has been found among X-ray selected galaxies and has been shown to have important consequences for the analysis of fainter X-ray samples (Gioia *et al.* 1984).

The present study focuses on a complete sample of galaxies brighter than 2 Jy at 60 $\mu$m. We have obtained redshift data for the entire sample by extending the redshift survey of optically selected galaxies carried out in this region by de Lapparent, Geller, and Huchra (1986). Accurate four-color infrared photometry of all objects in the sample was also obtained by using the *IRAS* survey data base. From these data, we have constructed a new 60 $\mu$m luminosity function and compare it to previous results obtained from other infrared flux-limited samples of galaxies. Finally, we compare the absolute blue magnitudes and nuclear activity of our sample with those of a blue-selected sample and exploit the spatial overlap between the optical survey and the present study to make a direct comparison of the space distribution of infrared-selected and blue-selected galaxies.

## II. THE SAMPLE

Our sample includes all sources listed in the *IRAS Point Source Catalog* (1985; hereafter PSC) above a flux limit of 2 Jy at 60 $\mu$m and lying within the 1072 square degree region between $8^h < \alpha < 17^h$, $23^\circ.5 < \delta < 32^\circ.5$. This region is at sufficiently high galactic latitude ($b > 20^\circ$) that confusion with galactic objects and infrared cirrus is minimized. Eighty-six sources met the selection criterion.

In order to minimize bias in the sample against nearby galaxies of large angular size, we searched the *IRAS* Small Scale Structures Catalog (1986; hereafter SSS) for additional objects. This catalog lists 14 objects with $S(60) > 2$ Jy in our region of sky. Of these, seven were slightly extended galaxies already in our sample, and six were found to be condensations in cirrus clouds (Low *et al.* 1984). The remaining source was identified with the nearby spiral galaxy NGC 4725. This galaxy was listed in the PSC, but because of its large angular extent ($\Theta \sim 9'$), its flux was underestimated in the PSC to be only 0.9 Jy at 60 $\mu$m. This object was added to our list, and accurate *IRAS* photometry was obtained from the *IRAS Atlas of Optically Large Galaxies* (Rice *et al.* 1986). As a further check on incompleteness due to large galaxies, we searched the *Uppsala General Catalog of Galaxies* (Nilson 1973). It lists 39 galaxies having $m_B < 13$ in the selected region; 21 are not in our

[1] Work reported here is based on observations obtained with the MMT, a joint facility of the Smithsonian Institution and the University of Arizona.

sample; all of these have angular sizes greater than the resolution of the PSC at 60 $\mu$m, $1' < \Theta_{BLUE} < 5'$. If their structures are similar to that of NGC 4725 then we expect that $F(60) < 1.5$ Jy for each of these galaxies; co-addition of the survey data in the vicinity of these sources can confirm that they are below the flux limit of our survey.

The selected sources are listed in Table 1. Optical and radio identifications were made on the basis of positional proximity. Thirteen of our sources are stars, one is a planetary nebula, and 72 are galaxies. Twenty-two of the galaxies in our sample were found to occur in groups of two or more. For these cases, we obtained accurate positions ($<1''$) on the two-axis Grant machine at NOAO.[2] Table 2 lists these sources, the parameters of their error ellipses from the PSC, and the positions of the optical counterparts. The first optical source listed is the assumed association with the *IRAS* source. In four cases, more than one optical object lies within the quoted error ellipse. In these cases the *IRAS* source was associated with the brightest galaxy.

## III. INFRARED PHOTOMETRY

Table 3 lists the *IRAS* name, the morphological classification, and the *IRAS* flux densities of all the sources in our sample. These data were obtained by co-adding all available *IRAS* data using the Add Scan Program at the Infrared Processing and Analysis Center.[3] For each unresolved source, the flux density was measured from the peak value in the median of all scans of each source. Detections with $3 < S/N < 5$ are indicated by a colon; 3 $\sigma$ upper limits are given for nondetections. Notes in the table indicate sources that were found to be extended in the infrared, such that the integrated flux exceeded that of a point source with the same peak flux by

[2] Operated by the Association of Universities for Research in Astronomy, Inc., under contract with the National Science Foundation.

[3] IPAC is funded by NASA as part of the *IRAS* extended mission program under contract to JPL.

TABLE 1

SELECTED SOURCES

| PSC Name | Other Names |
|---|---|
| 08001+2331 | NGC 2512, Mkn 384, ZG 800+23, UGC 04191, M+04-19-021 |
| 08082+2521 | NGC 2535, Arp 82, ZG 808+25, UGC 04264, M+04-20-004 |
| 08111+2401 | ZG 811+24, M+04-20-006 |
| 08117+2453 | RX Cnc, TMSS +20198, RAFGL 1240 |
| 08322+2838 | NGC 2608, ZG 832+28, UGC 04484, M+05-20-027 |
| 08323+3003 | |
| 08327+2855 | ZG 832+28 |
| 08354+2555 | NGC 2623, Arp 243, ZG 835+25, UGC 04509, M+04-21-009 |
| 09028+2538 | NGC 2750, ZG 902+25, UGC 04769, M+04-22-012 |
| 09069+2527 | W Cnc, TMSS +30208, RAFGL 1323 |
| 09076+3110 | RS Cnc, TMSS +30209, RAFGL 1326 |
| 09120+2956 | ZG 912+29, UGC 04875, M+05-22-026 |
| 09273+2945 | NGC 2893, Mkn 401, ZG 927+29, UGC 05060, M+05-23-005 |
| 09399+3204 | NGC 2964, Mkn 404, ZG 939+32, UGC 05183, M+05-23-027 |
| 09534+2727 | ZG 953+27, UGC 05335, M+05-24-003 |
| 10078+2439 | Mkn 717, ZG 1007+24, UGC 05488, M+04-24-016 |
| 10131+3049 | TMSS +30219, RAFGL 1403 |
| 10245+2845 | NGC 3245, ZG 1024+28, UGC 05663, M+05-25-013 |
| 10282+2903 | NGC 3265, M+05-25-019 |
| 10369+2659 | ZG 1036+27 |
| 10407+2511 | NGC 3344, M+04-25-046 |
| 10460+2619 | Mkn 727, M+04-26-009 |
| 10565+2448 | |
| 10576+2914 | NGC 3486, ZG 1057+29, UGC 06079, M+05-26-032 |
| 11004+2814 | NGC 3504, ZG 1100+28, UGC 06118, M+05-26-039 |
| 11069+2711 | |
| 11085+2859 | NGC 3561, Arp 105, ZG 1108+28, UGC 06224, M+05-27-011 |
| 11102+3026 | |
| 11474+2645 | NGC 3912, ZG 1147+26, UGC 06801, M+05-28-037 |
| 11547+2528 | NGC 3987, ZG 1154+25, UGC 06928, M+04-28-099 |
| 11555+2809 | NGC 4004, Mkn 432, M+05-28-059 |
| 11561+2535 | ZG 1156+25, UGC 06966, M+04-28-108 |
| 11561+2743 | ZG 1156+27, UGC 06967, M+05-28-065 |
| 11598+3008 | ZG 1159+30, UGC 07017, M+05-28-078 |
| 12015+3210 | NGC 4062, ZG 1201+32, UGC 07045, M+05-29-004 |
| 12021+3126 | ZG 1202+31, UGC 07064, M+05-29-005 |
| 12031+3120 | ZG 1203+31, UGC 07085A, M+05-29-010 |
| 12093+2423 | NGC 4162, ZG 1209+24, UGC 07193, M+04-29-046 |
| 12099+2926 | NGC 4175, Mkn 761, ZG 1210+29, UGC 07211, M+05-29-036 |
| 12159+3005 | NGC 4253, Mkn 766, ZG 1215+30, UGC 07344 |
| 12173+2953 | NGC 4274, ZG 1217+29, UGC 07377, M+05-29-060 |
| 12200+3010 | NGC 4314, ZG 1220+30, UGC 07443 |
| 12239+3129 | NGC 4414, ZG 1224+31, UGC 07539 |
| 12289+2924 | ZG 1228+29, M+05-30-012 |
| 12334+2814 | NGC 4559, ZG 1233+28, UGC 07766, M+05-30-030 |
| 12338+2615 | NGC 4565, ZG 1233+26, UGC 07772, M+04-30-006 |
| 12341+2442 | ZG 1234+24, M+04-30-009 |
| 12344+2720 | TMSS +30241, RAFGL 1564 |
| 12415+3226 | NGC 4656, ZG 1241+32, UGC 07907, M+05-30-066 |
| 12422+2641 | M+05-30-069 |
| 12428+2724 | NGC 4670, Arp 163, ZG 1242+27, UGC 07930, M+05-30-072 |
| 12437+3059 | NGC 4676A, Arp 242, ZG 1243+31, UGC 07938, M+05-30-077 |
| X1247+2547 | NGC 4725, M+04-30-022 |
| 12522+2912 | NGC 4793, ZG 1252+29, UGC 08033, M+05-31-003 |
| 12590+2934 | NGC 4922, ZG 1259+29, UGC 08135, M+05-31-099 |
| 13086+2950 | NGC 5004A, ZG 1308+29, UGC 08259, M+05-31-150 |
| 13126+2452 | ZG 1312+24, M+04-31-015 |
| 13376+2839 | ZG 1337+28UGC 08648, M+05-32-058 |
| 13387+2331 | ZG 1338+23, M+04-32-025 |
| 13408+3035 | ZG 1340+30, UGC 08685, M+05-32-074 |
| 13532+2517 | ZG 1353+25, M+04-33-027 |
| 13538+3019 | ZG 1353+30, UGC 08856, M+05-33-021 |
| 13573+2801 | WY Boo, TMSS +30253 |
| 14008+2816 | M+05-33-042 |
| 14026+3058 | ZG 1402+30, M+05-33-046 |
| 14151+2705 | Mkn 673, ZG 1415+27, UGC 09141, M+05-34-007 |
| 14158+2741 | |
| 14165+2510 | ZG 1416+25, UGC 09165, M+04-34-015 |
| 14219+2555 | RX Boo, TMSS +30257, RAFGL 1706 |
| 14221+2450 | ZG 1422+24, UGC 09230, M+04-34-025 |
| 14280+3126 | NGC 5653, ZG 1427+31, UGC 09318, M+05-34-058 |
| 14356+3041 | ZG 1435+30, UGC 09425, M+05-34-083 |
| 14390+3147 | RW Boo, TMSS +30262, RAFGL 1720 |
| 14547+2448 | Arp 302, M+04-35-019 |
| 15018+2417 | |
| 15193+3132 | S CrB, +30272, RAFGL 4990 |
| 15327+2849 | ZG 1532+28, UGC 09909, M+05-37-003 |
| 15327+2340 | Arp 220, ZG 1532+23, UGC 09913, M+04-37-005 |
| 15361+2441 | TMSS +20283, RAFGL 1790 |
| 15373+2506 | Mkn 860, ZG 1537+25, M+04-37-016 |
| 15465+2818 | R CrB, RAFGL 4219 |
| 15566+2657 | Mkn 492, ZG 1556+26 |
| 16081+2511 | RU Her, TMSS +30283, RAFGL 1832 |
| 16211+3057 | RY CrB, TMSS +30290, RAFGL 5044 |
| 16403+2510 | ZG 1640+25, UGC 10514, M+04-39-020 |
| 16423+2353 | NGC 6210 |

TABLE 2

*IRAS* AND OPTICAL POSITIONS OF SELECTED SOURCES

| PSC NAME | IRAS POSITION α | IRAS POSITION δ | AXES (") | | P.A. (DEG.) | | OPTICAL POSITIONS α | OPTICAL POSITIONS δ |
|---|---|---|---|---|---|---|---|---|
| 08082+2521 | 08 08 13.0 | 25 21 15 | 32 | 8 | 102 | A | 08 08 13.1 | 25 21 22 |
| | | | | | | B | 08 08 15.7 | 25 19 43 |
| 08322+2838 | 08 32 14.0 | 28 38 49 | 41 | 6 | 104 | A | 08 32 14.9 | 28 38 48 |
| | | | | | | B | 08 32 19.6 | 28 40 23 |
| 08323+3003 | 08 32 19.4 | 30 03 35 | 43 | 9 | 104 | A | 08 32 19.4 | 30 03 22 |
| | | | | | | B | 08 32 19.4 | 30 03 38 |
| | | | | | | C | 08 32 18.7 | 30 03 16 |
| 08354+2555 | 08 35 25.0 | 25 55 49 | 21 | 5 | 104 | A | 08 35 25.3 | 25 55 49 |
| | | | | | | B | 08 35 24.9 | 25 55 51 |
| | | | | | | C | 08 35 25.4 | 25 55 35 |
| | | | | | | D | 08 35 19.2 | 25 56 41 |
| | | | | | | E | 08 35 34.7 | 25 57 12 |
| 10565+2448 | 10 56 35.4 | 24 48 43 | 34 | 7 | 114 | A | 10 56 36.1 | 24 48 40 |
| 11069+2711 | 11 06 56.9 | 27 11 23 | 28 | 7 | 115 | A | 11 06 56.1 | 27 11 32 |
| | | | | | | B | 11 06 57.5 | 27 11 13 |
| | | | | | | C | 11 06 56.4 | 27 11 11 |
| | | | | | | D | 11 06 58.7 | 27 10 57 |
| 11102+3026 | 11 10 15.5 | 30 26 47 | 34 | 7 | 117 | A | 11 10 15.6 | 30 26 49 |
| 11555+2809 | 11 55 30.9 | 28 09 19 | 21 | 10 | 116 | A | 11 55 31.1 | 28 09 25 |
| | | | | | | B | 11 55 17.2 | 28 08 49 |
| 12021+3126 | 12 02 10.0 | 31 26 50 | 31 | 10 | 116 | A | 12 02 10.3 | 31 27 20 |
| | | | | | | B | 12 02 12.1 | 31 26 15 |
| | | | | | | C | 12 02 12.1 | 31 28 15 |
| | | | | | | D | 12 02 12.6 | 31 28 08 |
| 12031+3120 | 12 03 11.0 | 31 20 16 | 36 | 10 | 117 | A | 12 03 12.6 | 31 20 08 |
| | | | | | | B | 12 03 12.6 | 31 21 27 |
| | | | | | | C | 12 03 17.8 | 31 19 35 |
| 12437+3059 | 12 43 46.0 | 31 00 00 | 24 | 10 | 119 | A | 12 43 45.4 | 30 59 47 |
| | | | | | | B | 12 43 44.1 | 31 00 19 |
| 12590+2934 | 12 59 01.0 | 29 34 58 | 47 | 8 | 115 | B | 12 59 0.4 | 29 34 37 |
| | | | | | | A | 12 59 1.0 | 29 34 59 |
| | | | | | | C | 12 58 58.0 | 29 36 31 |
| 13086+2950 | 13 08 38.0 | 29 50 38 | 50 | 11 | 115 | A | 13 08 39.4 | 29 50 37 |
| | | | | | | B | 13 08 39.3 | 29 54 09 |
| 13532+2517 | 13 53 15.0 | 25 17 41 | 33 | 10 | 112 | A | 13 53 15.7 | 25 17 39 |
| | | | | | | B | 13 53 13.8 | 25 19 8 |
| 13538+3019 | 13 53 52.0 | 30 19 42 | 42 | 8 | 116 | A | 13 53 53.0 | 30 19 32 |
| | | | | | | B | 13 53 55.3 | 30 20 30 |
| 14151+2705 | 14 15 06.0 | 27 05 17 | 35 | 10 | 112 | A | 14 15 04.0 | 27 05 25 |
| | | | | | | B | 14 15 06.1 | 27 05 14 |
| 14158+2714 | 14 15 48.9 | 27 41 48 | 37 | 11 | 114 | A | 14 15 49.1 | 27 41 49 |
| | | | | | | B | 14 15 48.8 | 27 41 56 |
| | | | | | | C | 14 15 48.8 | 27 41 32 |
| 14356+3041 | 14 35 40.0 | 30 41 57 | 20 | 13 | 107 | A | 14 35 41.6 | 30 41 56 |
| | | | | | | B | 14 35 42.3 | 30 41 43 |
| 14547+2448 | 14 54 47.9 | 24 48 57 | 20 | 10 | 107 | B | 14 54 48.3 | 24 49 03 |
| | | | | | | A | 14 54 47.9 | 24 48 24 |
| | | | | | | C | 14 54 47.8 | 24 48 42 |
| 15018+2417 | 15 01 49.1 | 24 17 53 | 25 | 9 | 104 | A | 15 01 48.5 | 24 17 56 |
| | | | | | | D | 15 01 47.6 | 24 17 56 |
| | | | | | | C | 15 01 50.9 | 24 17 38 |
| | | | | | | E | 15 01 48.5 | 24 17 15 |
| | | | | | | F | 15 01 53.5 | 24 16 57 |
| 15327+2340 | 15 32 46.0 | 23 40 10 | 17 | 9 | 104 | A | 15 32 46.6 | 23 40 11 |
| | | | | | | B | 15 32 47.4 | 23 40 26 |
| | | | | | | C | 15 32 46.8 | 23 39 59 |
| 15373+2506 | 15 37 18.0 | 25 06 28 | 24 | 8 | 103 | A | 15 37 19.2 | 25 06 32 |
| | | | | | | B | 15 37 17.7 | 25 06 17 |

TABLE 3

CLASSIFICATIONS AND CORRECTED *IRAS* PHOTOMETRY

| Name | Type | $F_{12}$ | $F_{25}$ | $F_{60}$ | $F_{100}$ | Notes |
|---|---|---|---|---|---|---|
| 08001+2331 | SBb | 0.31 ( 21) | 0.65 ( 5) | 4.05 ( 8) | 8.31 ( 1) | |
| 08082+2521 | Sc P | 0.16: ( 20) | 0.32 ( 6) | 4.05 ( 9) | 7.63 ( 1) | 3, 4, 7, 9 |
| 08111+2401 | E | 0.24 ( 22) | 0.52 ( 5) | 3.00 ( 8) | 6.61 ( 1) | |
| 08117+2453 | star | 28.4 (-22) | 9.36 (-26) | 1.88 (-22) | 1.24 (-5) | |
| 08322+2838 | S | 0.28 ( 13) | 0.39 ( 0) | 2.46 ( 9) | 6.77 ( 3) | |
| 08323+3003 | triple | <0.11 ( 20) | 0.16: ( 2) | 3.24 ( 11) | 4.75 ( -4) | |
| 08327+2855 | S | 0.19: ( 22) | 0.37 ( 4) | 2.39 ( 6) | 3.67 ( -1) | |
| 08354+2555 | pair | 0.40 ( 29) | 2.20 ( 17) | 25.6 ( 7) | 27.9 ( -3) | |
| 09028+2538 | Sc | <0.21 ( 24) | 0.63 ( 9) | 4.24 ( 8) | 8.63 ( 2) | |
| 09069+2527 | star | 73.5 (-17) | 27.9 (-24) | 4.63 (-20) | 2.55 ( -6) | |
| 09076+3110 | star | 399. (-14) | 165.0 (-23) | 26.0 (-21) | 11.1 ( -7) | |
| 09120+2956 | S0/a | 0.29 ( 16) | 0.44 ( 0) | 2.22 ( 7) | 5.94 ( 2) | |
| 09273+2945 | SB0/a | 0.27 ( 22) | 0.69 ( 6) | 2.63 ( 5) | 3.99 ( 0) | |
| 09399+3204 | SABbc | 0.84 ( 20) | 1.79 ( 5) | 12.8 ( 8) | 27.7 ( 2) | 1, 2 |
| 09534+2727 | Im | 0.30 ( 16) | 0.50 ( 2) | 3.79 ( 8) | 7.95 ( 2) | |
| 10078+2439 | S | 0.29 ( 27) | 0.88 ( 8) | 3.78 ( 3) | 4.15 ( -4) | |
| 10131+3049 | star | 2890. (-21) | 987. (-25) | 211. ( 22) | 91.8 ( -7) | |
| 10245+2845 | S0 | 0.17: ( 9) | 0.20: ( -2) | 2.34 ( 9) | 4.22 ( 1) | |
| 10282+2903 | E | 0.16 ( 22) | 0.45 ( 8) | 2.58 ( 7) | 4.12 ( 1) | 2 |
| 10369+2659 | S | 0.32 ( 14) | 0.43 (-1) | 3.43 ( 8) | 6.69 ( 1) | |
| 10407+2511 | Sbc | 1.94 ( 14) | 2.69 ( 0) | 9.49 ( 7) | 29.1 ( 3) | 1, 2, 3, 4, 5, 6, 7 |
| 10460+2619 | cI | 0.16: ( 31) | 0.70 ( 11) | 2.32 ( 1) | 2.48 ( -5) | |
| 10565+2448 | Im | 0.25 ( 40) | 1.56 ( 21) | 12.8 ( 7) | 16.4 ( -4) | |
| 10576+2914 | SABc | 0.35 ( -4) | 0.24 ( -9) | 7.70 ( 10) | 17.4 ( 2) | 1, 2, 3, 4, 7 |
| 11004+2814 | SABab | 1.45 ( 23) | 4.37 ( 8) | 23.4 ( 7) | 39.3 ( 1) | |
| 11069+2711 | pair | <0.10 ( 16) | 0.14: ( -2) | 2.56 ( 12) | 4.59 ( -3) | |
| 11085+2859 | Sa | <0.16 ( 33) | 0.70 ( 14) | 4.38 ( 8) | 8.22 ( 0) | |
| 11102+3026 | S | <0.09 ( 14) | 0.12: ( 0) | 2.39 ( 11) | 4.43 ( 0) | |
| 11474+2645 | SABb | 0.27 ( 18) | 0.49 ( 3) | 3.48 ( 9) | 7.67 ( 2) | |
| 11547+2528 | Sb | 0.32 ( 15) | 0.47 ( 1) | 5.30 ( 11) | 16.5 ( 4) | 1, 2, 3 |
| 11555+2809 | SBdm P | 0.23 ( 21) | 0.50 ( 6) | 3.92 ( 8) | 7.72 ( 1) | |
| 11561+2535 | Sab | 0.26 ( 8) | 0.27 ( -4) | 2.47 ( 9) | 6.59 ( 3) | 1, 2 |
| 11561+2743 | SABbc | 0.22 ( 4) | 0.20 ( -6) | 2.35 ( 10) | 6.15 ( 3) | |
| 11598+3008 | Sb | 0.37 ( 4) | 0.34 ( -6) | 3.89 ( 9) | 8.50 ( 2) | |
| 12015+3210 | Sc | 0.35 ( 4) | 0.32 ( -5) | 2.84 ( 10) | 12.6 ( 4) | 1, 2, 3, 4 |
| 12021+3126 | pair S | 0.20: ( 32) | 1.05 ( 13) | 3.46 ( 5) | 6.93 ( 0) | 1, 2, 3 |
| 12031+3120 | S0- | <0.11 ( 27) | 0.33 ( 9) | 2.19 ( 6) | 2.79 ( -3) | |
| 12093+2423 | Sbc | 0.24 ( -2) | 0.17 ( -9) | 2.56 ( 10) | 7.44 ( 3) | 1, 2, 3 |
| 12099+2926 | Sab | 0.38 ( 16) | 0.58 ( 2) | 5.79 ( 9) | 2.78 ( 2) | |
| 12159+3005 | SBa | 0.50 ( 26) | 1.71 ( 7) | 4.00 ( 1) | 5.04 ( -2) | |
| 12173+2953 | SBab | 0.38 ( 13) | 0.52 ( 0) | 4.45 ( 10) | 17.2 ( 4) | 1, 2 |
| 12200+3010 | SBa | 0.25 ( 20) | 0.54 ( 6) | 3.96 ( 9) | 9.12 ( 2) | |
| 12239+3129 | Sc | 3.19 ( 10) | 3.72 ( -2) | 29.3 ( 9) | 83.1 ( 3) | 1, 2, 3, 4 |
| 12289+2924 | Sab | 0.28 ( 20) | 0.52 ( 3) | 3.29 ( 8) | 7.62 ( 2) | |
| 12334+2814 | SABcd | 0.89 ( 8) | 0.96 ( -2) | 12.0 ( 9) | 25.8 ( 2) | 1, 2, 3, 4, 7 |
| 12338+2615 | Sb | 2.58 ( -8) | 1.48 (-13) | 11.78 ( 9) | 38.3 ( 3) | 1, 2, 3, 5, 6, 7 |
| 12341+2442 | Scd | 0.27 ( 18) | 0.45 ( 2) | 4.06 ( 7) | 5.72 ( -2) | |
| 12344+2720 | star | 65.8 (-10) | 31.9 (-21) | 4.60 (-19) | 2.29 ( -6) | |
| 12415+3226 | SBm | <0.26 ( 17) | 0.45 ( 5) | 9.05 ( 9) | 12.9 ( 0) | 2, 3, 4, 10 |
| 12422+2641 | S | 0.15: ( 26) | 0.50 ( 10) | 3.39 ( 7) | 5.59 ( 0) | |
| 12428+2724 | cI | 0.15: ( 21) | 0.38 ( 8) | 3.08 ( 8) | 5.25 ( 1) | |
| 12437+3059 | Sb0/a | 0.18 ( 26) | 0.47 ( 8) | 2.95 ( 8) | 5.58 ( 0) | 2 |
| X1247+2547 | SABb | 0.78 ( 4) | 0.69 ( -6) | 5.02 ( 9) | 22.0 ( 4) | 1, 2, 3, 4, 11 |
| 12522+2912 | SABc | 1.22 ( 13) | 1.63 ( 0) | 12.5 ( 9) | 32.7 ( 3) | 1, 2 |
| 12590+2934 | P | 0.38 ( 30) | 1.59 ( 12) | 6.45 ( 4) | 7.99 ( -3) | |
| 13086+2950 | SBab | <0.16 ( 15) | 0.23 ( 0) | 2.28 ( 9) | 4.49 ( 1) | |
| 13126+2452 | S | <0.11 ( 19) | 1.77 ( 23) | 19.0 ( 6) | 19.1 ( -3) | |
| 13376+2839 | Sc | 0.26 ( 13) | 0.35 ( 0) | 3.74 ( 10) | 8.96 ( 2) | 1 |
| 13387+2331 | pair | 0.26 ( 30) | 0.89 ( 11) | 4.85 ( 6) | 7.18 ( -2) | |
| 13408+3035 | SBb | 0.20 ( 25) | 0.42 ( 5) | 2.59 ( 8) | 5.99 ( 1) | |
| 13532+2517 | | <0.17 ( 28) | 0.44 ( 7) | 2.26 ( 4) | 2.75 ( -4) | |
| 13538+3019 | Sc | 0.20: ( 10) | 0.22 ( -4) | 2.57 ( 10) | 5.16 ( 0) | 3, 12 |
| 13573+2801 | star | 21.0 ( -7) | 11.1 (-20) | 1.80 (-18) | 0.94 ( -6) | |
| 14008+2816 | S | 0.18: ( 20) | 0.34 ( 4) | 2.27 ( 8) | 4.82 ( 2) | 1, 2 |
| 14026+3058 | Scd | <0.13 ( 29) | 0.40 ( 11) | 2.97 ( 8) | 5.14 ( 0) | |
| 14151+2705 | S | 0.20 ( 23) | 0.38 ( 4) | 3.01 ( 9) | 6.06 ( 0) | |
| 14158+2741 | | <0.10 ( 19) | 0.14: ( 1) | 2.60 ( 12) | 4.37 ( -3) | |
| 14165+2510 | S | 0.25 ( 19) | 0.43 ( 3) | 3.57 ( 9) | 8.16 ( 2) | |
| 14219+2555 | star | 738. (-14) | 291. (-27) | 53.7 (-23) | 27.2 ( -6) | |
| 14221+2450 | SBa | 0.35 ( 25) | 0.95 ( 8) | 5.40 ( 7) | 9.02 ( 0) | |

TABLE 3—*Continued*

| Name | Type | $F_{12}$ | $F_{25}$ | $F_{60}$ | $F_{100}$ | Notes |
|---|---|---|---|---|---|---|
| 14280+3126 | Sb | 0.84 ( 20) | 1.61 ( 4) | 11.9 ( 8) | 25.1 ( 1) | |
| 14356+3041 | pair P | 0.20: ( 31) | 0.57 ( 8) | 2.52 ( 4) | 3.46 ( -3) | |
| 14390+3147 | star | 54.4 (-12) | 22.5 (-26) | 4.24 (-23) | 3.16 ( -4) | |
| 14547+2448 | pair | 0.33 ( 21) | 0.57 ( 4) | 7.04 ( 11) | 16.7 ( 2) | |
| 15018+2417 | | <0.11 ( 43) | 0.38 ( 14) | 3.05 ( 6) | 4.16 ( -6) | |
| 15193+3132 | star | 199. ( -9) | 97.6 (-21) | 15.3 (-19) | 7.10 ( -7) | |
| 15327+2849 | Sc | 0.14: ( 17) | 0.25 ( 4) | 2.66 ( 9) | 5.74 ( 2) | |
| 15327+2340 | P | 0.70 ( 23) | 11.0 ( 25) | 111. ( 7) | 126. ( -3) | |
| 15361+2441 | star | 66.4 (-26) | 19.5 (-27) | 3.19 (-22) | 1.69 ( -6) | |
| 15373+2506 | pair S | 0.14: ( 31) | 0.71 ( 12) | 2.38 ( 3) | 3.39 ( -2) | |
| 15465+2818 | star | 33.5 (-13) | 14.2 (-23) | 3.31 (-19) | 2.40 ( -4) | |
| 15566+2657 | S | 0.20: ( 27) | 0.95 ( 11) | 3.26 ( 2) | 3.43 ( -3) | |
| 16081+2511 | star | 156. (-15) | 64.0 (-23) | 9.14 (-20) | 4.90 ( -6) | |
| 16211+3057 | star | 23.9 ( -7) | 11.5 (-26) | 2.16 (-23) | 1.43 ( -5) | |
| 16403+2510 | Sd | <0.15 ( 25) | 0.37 ( 8) | 2.91 ( 8) | 5.29 ( 0) | |
| 16423+2353 | Plan. Neb. | 2.37 ( 13) | 30.6 ( 10) | 32.1 (-10) | 16.0 ( -6) | |

NOTES.—(1) Extended in Band 1; (2) Extended in Band 2; (3) Extended in Band 3; (4) Extended in Band 4; (5) Flux in Band 1 from SSS; (6) Flux in Band 2 from SSS; (7) Flux in Band 3 from SSS; (8) Flux in Band 4 from SSS; (9) Double, 1.'5 separation, fluxes combined; (10) Double, 3' separation, fluxes combined; (11) Fluxes derived by W. Rice from *IRAS* Add-Scan data; (12) Double, 1.'1 separation, fluxes combined.

more than 15%. We used data from the SSS for these sources, where it was available; otherwise, we integrated the median scan generated by Add-Scan to obtain the result.

Both color corrections and $K$-corrections have been applied to the data listed in Table 1. These corrections were deduced using the method described in the Appendix. Table 3 also includes the percentage correction made to the *IRAS* flux density. Application of these corrections raises the flux density of the faintest source included in our sample to 2.3 Jy.

As can be seen in Figure 1, galactic and extragalactic objects show dramatic segregation by infrared colors. The flux densities observed for the stars decrease with increasing wavelength, while the flux densities of the galaxies increase with increasing wavelength. The galaxies in this sample have $F(60) > 2F(25)$ and $F(100) > F(60)$, while the stars have $F(12) > 3F(25)$, $F(25) > 2.5F(60)$, $F(60) > F(100)$. For galaxies,

$$\left\langle \frac{F_{60}}{F_{25}} \right\rangle = 9.0 \pm 5.4$$

$$\left\langle \frac{F_{100}}{F_{60}} \right\rangle = 2.0 \pm 0.7 ,$$

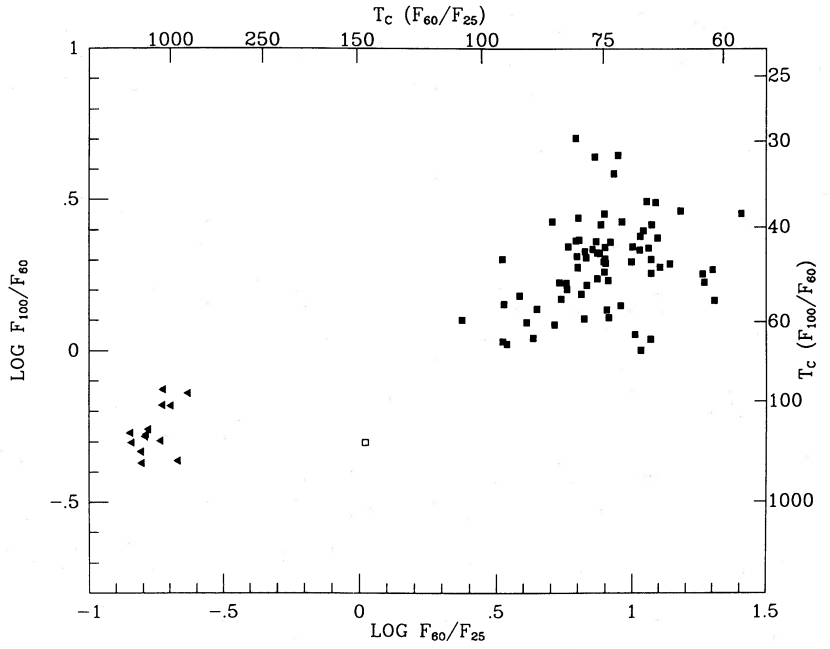


FIG. 1.—Color distribution of all selected sources. Galaxies are represented by triangles, stars by filled squares, and the planetary nebula by the unfilled square. The fluxes have been color corrected and $K$-corrected assuming the spectral energy distribution can be approximated by a blackbody (see Appendix).

TABLE 4

SPECTROSCOPIC RESULTS AND DERIVED LUMINOSITIES

| Name | Equivalent Widths (magnitudes) | | | | | $m_B$ | $v_h$ | $\sigma_v$ | log $L_B$ | log $L_{60}$ |
|---|---|---|---|---|---|---|---|---|---|---|
| | Hα | Hβ | λ5007 | λ6584 | λ6300 | | | | | |
| 08001+2331 | | | | | | 14.2 | 4647 | 53 | 9.6 | 10.0 |
| 08082+2521 | -0.89 (.09) | -0.01 (.11) | -0.33 (.12) | -0.5 (.1) | 0.04 (.09) | 13.5 | 4104 | 37 | 9.8 | 9.9 |
| 08111+2401 | -0.43 (.05) | -0.05 (.04) | -0.08 (.04) | -0.35 (.05) | 0.01 (.04) | 15.3 | 6052 | 27 | 9.4 | 10.1 |
| 08322+2838 | -0.79 (.06) | -0.15 (.06) | -0.07 (.07) | -0.48 (.06) | -0.05 (.06) | 12.9 | 2126 | 32 | 9.4 | 9.2 |
| 08323+3003 | 0.4 (.1) | 0.43 (.14) | 0.00 (.14) | -0.19 (.22) | 0.32 (.19) | 18.0 | 17885 | 38 | 9.2 | 11.1 |
| 08327+2855 | -0.57 (.04) | 0.01 (.05) | -0.02 (.05) | -0.48 (.04) | -0.08 (.04) | 15.3 | 7621 | 29 | 9.6 | 10.2 |
| 08354+2555 | -0.41 (.05) | 0.13 (.06) | 0.03 (.05) | -0.36 (.05) | -0.14 (.04) | 14.4 | 5508 | 27 | 9.6 | 11.0 |
| 09028+2538 | -1.60 (.04) | -0.43 (.04) | -0.08 (.04) | -0.89 (.04) | -0.01 (.04) | 12.7 | 2670 | 31 | 9.7 | 9.6 |
| 09120+2956 | -0.49 (.06) | 0.10 (.03) | -0.01 (.04) | -0.39 (.06) | 0.03 (.05) | 13.8 | 6313 | 29 | 10.0 | 10.0 |
| 09273+2945 | -1.08 (.05) | -0.23 (.03) | -0.07 (.03) | -0.71 (.05) | -0.14 (.04) | 13.6 | 1678 | 31 | 9.0 | 9.0 |
| 09399+3204 | -1.22 (.06) | -0.16 (.04) | -0.16 (.04) | -0.76 (.06) | -0.14 (.05) | 12.4 | 1353 | 31 | 9.3 | 9.6 |
| 09534+2727 | -1.18 (.05) | -0.23 (.03) | -0.29 (.03) | -0.67 (.06) | -0.01 (.05) | 14.3 | 1236 | 32 | 8.5 | 8.9 |
| 10078+2439 | -2.09 (.06) | -0.72 (.06) | -0.58 (.07) | -1.43 (.06) | -0.16 (.06) | 14.6 | 6365 | 30 | 9.7 | 10.3 |
| 10245+2845 | -0.02 (.02) | -0.02 (.02) | 0.03 (.03) | -0.02 (.02) | -0.01 (.02) | 12.0 | 1370 | 19 | 9.5 | 8.9 |
| 10282+2903 | -1.46 (.06) | -0.39 (.02) | -0.21 (.02) | -0.70 (.06) | -0.11 (.04) | 14.1 | 1429 | 28 | 8.7 | 8.9 |
| 10369+2659 | -1.37 (.07) | -0.5 (.1) | -0.14 (.09) | -0.87 (.08) | -0.17 (.07) | 15.1 | 5844 | 32 | 9.4 | 10.2 |
| 10407+2511 | -0.69 (.03) | -0.17 (.03) | -0.25 (.03) | -0.33 (.03) | -0.02 (.03) | 11.1 | 582 | 27 | 9.2 | 8.9 |
| 10460+2619 | -2.68 (.05) | -1.13 (.04) | -1.92 (.04) | -1.02 (.06) | -0.24 (.05) | 15.7 | 7687 | 34 | 9.4 | 10.2 |
| 10565+2448 | -1.78 (.07) | -0.38 (.03) | -0.14 (.04) | -1.12 (.08) | -2.0 (.06) | 16.0 | 12926 | 36 | 9.7 | 11.4 |
| 10576+2914 | 0.14 (.04) | 0.11 (.05) | -0.17 (.05) | 0.02 (.04) | -0.02 (.04) | 11.1 | 679 | 10 | 9.4 | 8.8 |
| 11004+2814 | -1.5 (.03) | -0.37 (.03) | -0.25 (.04) | -1.06 (.03) | -0.08 (.03) | 11.8 | 1530 | 32 | 9.7 | 9.9 |
| 11069+2711 | -1.6 (.7) | -0.35 (.05) | -0.16 (.06) | -1.1 (.2) | -0.21 (.10) | 17.0 | 21080 | 40 | 9.8 | 11.2 |
| 11085+2859 | | | | | | 14.7 | 8556 | 34 | 9.9 | 10.6 |
| 11102+3026 | | | | | | 16.0 | 8788 | 28 | 9.4 | 10.4 |
| 11474+2645 | -1.05 (.06) | -0.25 (.07) | -0.15 (.08) | -0.40 (.07) | -0.14 (.07) | 13.0 | 1737 | 31 | 9.3 | 9.3 |
| 11547+2528 | -0.11 (.07) | -0.09 (.09) | 0.02 (.09) | 0.05 (.08) | 0.04 (.07) | 14.4 | 4543 | 38 | 9.5 | 10.2 |
| 11555+2809 | -1.86 (.09) | -0.66 (.08) | -0.57 (.08) | -0.75 (.09) | -0.22 (.08) | 14.0 | 3402 | 35 | 9.4 | 9.8 |
| 11561+2535 | -0.67 (.09) | -0.16 (.13) | -0.23 (.12) | -0.4 (.1) | -0.1 (.1) | 14.7 | 4468 | 37 | 9.4 | 9.8 |
| 11561+2743 | -0.93 (.09) | -0.14 (.07) | -0.07 (.08) | -0.35 (.09) | 0.02 (.08) | 13.5 | 3432 | 32 | 9.6 | 9.6 |
| 11598+3008 | -1.30 (.07) | -0.26 (.05) | -0.16 (.05) | -0.58 (.08) | -0.10 (.05) | 14.4 | 3174 | 23 | 9.2 | 9.7 |
| 12015+3210 | -0.05 (.07) | 0.12 (.05) | 0.08 (.05) | -0.05 (.07) | 0.03 (.06) | 12.2 | 776 | 36 | 9.1 | 8.6 |
| 12021+3126 | -0.77 (.05) | -0.12 (.05) | -1.25 (.05) | -0.65 (.05) | -0.21 (.05) | 14.0 | 7517 | 30 | 10.1 | 10.4 |
| 12031+3120 | -1.5 (.1) | -0.2 (.1) | -0.2 (.1) | -1.1 (.1) | -0.15 (.09) | 15.1 | 6910 | 37 | 9.6 | 10.1 |
| 12093+2423 | -0.24 (.05) | 0.02 (.07) | -0.04 (.07) | -0.11 (.05) | 0.06 (.05) | 12.8 | 2568 | 27 | 9.7 | 9.4 |
| 12099+2926 | -0.35 (.07) | 0.13 (.03) | -0.04 (.03) | -0.35 (.07) | -0.07 (.05) | 14.2 | 4034 | 31 | 9.5 | 10.1 |
| 12159+3005 | -1.15 (.02) | -0.81 (.01) | -1.97 (.01) | -1.20 (.02) | -0.16 (.02) | 13.7 | 3876 | 16 | 9.7 | 9.9 |
| 12173+2953 | 0.01 (.16) | 0.01 (.04) | 0.03 (.05) | 0.05 (.16) | 0.03 (.05) | 11.5 | 920 | 19 | 9.5 | 8.9 |
| 12200+3010 | -0.17 (.04) | 0.05 (.05) | 0.07 (.05) | -0.15 (.04) | -0.02 (.04) | 11.6 | 1004 | 28 | 9.5 | 8.9 |
| 12239+3129 | | | | | | 11.2 | 720 | 20 | 9.4 | 9.6 |
| 12289+2924 | -0.95 (.06) | -0.06 (.05) | -0.10 (.05) | -0.63 (.07) | -0.12 (.05) | 14.1 | 4572 | 30 | 9.6 | 10.0 |
| 12334+2814 | 0.25 (.01) | 0.38 (.11) | 0.16 (.09) | 0.00 (.08) | 0.01 (.07) | 10.6 | 816 | 10 | 9.8 | 9.3 |
| 12338+2615 | 0.05 (.04) | 0.09 (.05) | 0.06 (.05) | 0.07 (.04) | -0.02 (.04) | 10.6 | 1227 | 10 | 10.0 | 9.5 |
| 12341+2442 | 0.04 (.06) | 0.23 (.04) | -0.15 (.04) | -0.28 (.05) | -0.00 (.04) | 14.9 | 6920 | 20 | 9.7 | 10.4 |
| 12415+3226 | -3.45 (.15) | -1.73 (.13) | -2.99 (.13) | -0.37 (.27) | -0.4 (.2) | 11.2 | 649 | 7 | 9.4 | 9.0 |
| 12422+2641 | -0.93 (.07) | -0.20 (.09) | -0.15 (.09) | -0.69 (.07) | -0.06 (.07) | 15.3 | 4544 | 19 | 9.1 | 10.0 |
| 12428+2724 | -2.08 (.03) | -0.76 (.02) | -1.40 (.02) | -0.50 (.03) | -0.11 (.03) | 13.4 | 1051 | 29 | 8.8 | 8.8 |
| 12437+3059 | -0.38 (.06) | -0.03 (.03) | -0.06 (.04) | -0.22 (.06) | -0.06 (.04) | 14.8 | 6517 | 27 | 9.6 | 10.2 |
| X1247+2547 | | | | | | 10.0 | 1213 | 9 | 10.3 | 9.1 |
| 12522+2912 | -0.59 (.06) | -0.04 (.07) | 0.09 (.07) | -0.16 (.07) | -0.05 (.07) | 12.9 | 2453 | 30 | 9.6 | 10.1 |
| 12590+2934 | -1.49 (.04) | -0.46 (.06) | -1.08 (.06) | -1.20 (.04) | -0.26 (.04) | 15.0 | 7044 | 33 | 9.6 | 10.6 |
| 13086+2950 | -1.11 (.10) | -0.02 (.08) | 0.09 (.09) | -0.67 (.10) | -0.20 (.08) | 15.3 | 7252 | 44 | 9.5 | 10.2 |
| 13126+2452 | 0.12 (.10) | 0.25 (.11) | 0.12 (.10) | -0.10 (.09) | 0.12 (.10) | 14.8 | 3878 | 35 | 9.2 | 10.6 |
| 13376+2839 | -0.80 (.05) | -0.11 (.06) | -0.03 (.06) | -0.35 (.05) | 0.01 (.06) | 14.0 | 4848 | 33 | 9.7 | 10.1 |
| 13387+2331 | -1.36 (.14) | -0.14 (.07) | -0.49 (.06) | -1.43 (.14) | -0.49 (.06) | 15.1 | 8186 | 43 | 9.7 | 10.6 |
| 13408+3035 | -0.41 (.08) | -0.04 (.07) | -0.02 (.07) | -0.20 (.08) | 0.02 (.07) | 14.5 | 10407 | 35 | 10.2 | 10.6 |
| 13532+2517 | -0.30 (.13) | -0.01 (.11) | -0.05 (.12) | -0.24 (.14) | 0.06 (.11) | 15.5 | 8856 | 48 | 9.6 | 10.4 |
| 13538+3019 | -1.31 (.15) | -0.21 (.12) | -0.29 (.14) | -0.79 (.16) | -0.33 (.16) | 15.6 | 9274 | 50 | 9.6 | 10.5 |
| 14008+2816 | -0.39 (.04) | 0.00 (.05) | -0.06 (.05) | -0.36 (.4) | 0.06 (.11) | 14.7 | 4560 | 27 | 9.4 | 9.8 |
| 14026+3058 | -0.50 (.08) | -0.02 (.08) | -0.07 (.08) | -0.38 (.08) | -0.10 (.07) | 15.5 | 7578 | 35 | 9.5 | 10.4 |
| 14151+2705 | -0.46 (.06) | 0.16 (.03) | -0.04 (.04) | -0.44 (.07) | -0.06 (.06) | 15.0 | 10987 | 40 | 10.0 | 10.7 |
| 14158+2741 | -0.29 (.12) | 0.13 (.09) | -0.12 (.09) | -0.34 (.12) | 0.03 (.09) | 16.0 | 20902 | 39 | 10.2 | 11.2 |
| 14165+2510 | -0.56 (.08) | -0.19 (.11) | -0.01 (.12) | -0.42 (.08) | -0.05 (.08) | 15.3 | 5278 | 36 | 9.3 | 10.1 |
| 14221+2450 | -0.73 (.05) | 0.02 (.05) | -0.08 (.05) | -0.73 (.05) | -0.05 (.05) | 14.5 | 5087 | 26 | 9.6 | 10.3 |
| 14280+3126 | -0.85 (.05) | 0.03 (.06) | -0.03 (.06) | -0.35 (.05) | -0.04 (.04) | 13.4 | 3582 | 29 | 9.7 | 10.3 |
| 14356+3041 | -1.46 (.14) | -0.4 (.1) | 0.05 (.10) | -0.92 (.14) | -0.2 (.1) | 15.0 | 10408 | 33 | 10.0 | 10.5 |
| 14547+2448 | -1.23 (.14) | -0.16 (.05) | -0.13 (.06) | -0.54 (.15) | -0.00 (.08) | 14.6 | 10166 | 31 | 10.1 | 11.0 |
| 15018+2417 | -0.99 (.17) | -0.19 (.07) | -0.29 (.09) | -0.78 (.17) | -0.02 (.14) | 16.5 | 20685 | 47 | 9.9 | 11.2 |
| 15327+2849 | -1.44 (.07) | -0.41 (.04) | -0.49 (.04) | 0.66 (.08) | -0.04 (.06) | 13.2 | 2021 | 36 | 9.4 | 9.3 |
| 15327+2340 | -0.52 (.09) | -0.07 (.11) | -0.12 (.10) | -0.57 (.09) | -0.04 (.08) | 14.4 | 5563 | 37 | 9.7 | 11.7 |
| 15373+2506 | -1.63 (.27) | -0.68 (.13) | -1.44 (.13) | -0.62 (.28) | -0.13 (.26) | 15.1 | 6869 | 37 | 9.6 | 10.2 |
| 15566+2657 | -1.44 (.05) | -0.23 (.05) | -0.20 (.05) | -0.98 (.05) | -0.04 (.04) | 14.9 | 4265 | 35 | 9.3 | 9.9 |
| 16403+2510 | -2.14 (.14) | -0.55 (.11) | -1.02 (.11) | -1.07 (.14) | -0.24 (.14) | 15.4 | 6783 | 35 | 9.4 | 10.2 |

where the quoted uncertainties are the rms dispersion about the average. For the stars in our sample,

$$\left\langle \frac{F_{60}}{F_{25}} \right\rangle = 0.17 \pm 0.03$$

$$\left\langle \frac{F_{100}}{F_{60}} \right\rangle = 0.56 \pm 0.10 .$$

One planetary nebula is included in this sample; it has an intermediate spectrum, with $F(60) > F(25)$, but $F(100) < F(60)$.

## IV. OPTICAL OBSERVATIONS

Spectra with a resolution of 6–7 Å covering 4600–7200 Å were obtained at the F. L. Whipple 1.5 m telescope and at the MMT using a photon-counting Reticon system (Latham 1982). The slit sizes used are 3.″2 × 6.″4 at the 1.5 m and 1.″0 × 3.″0 at the MMT. Several galaxies were observed in the confused cases; all our pairs appear to be physically associated, i.e., at the same redshift. Table 4 lists the galaxies in our sample with the equivalent widths of the Hα, Hβ, [O III] λ5007, [O I] λ6300, and [N II] λ6585 lines. Columns (7), (8), and (9) give the apparent blue magnitude, the heliocentric recessional velocity, and the uncertainty in the velocity. For galaxies brighter than $m_B = 15.7$, the magnitudes were taken from the Zwicky Catalog (Zwicky *et al.* 1961); these are accurate to 0.3 mag (Huchra 1976). For the six galaxies not in Zwicky's list, eye estimates were made by one of us (J. P. H); these were checked by determining the correlation between size and apparent magnitude for the brighter galaxies, and, assuming the same "surface brightness" for the fainter galaxies, using their angular sizes to estimate their brightness. This process showed that the eye estimates were typically accurate to 0.5 mag.

The redshift distribution of our sample is shown in Figure 2. The maximum redshift of 0.07 corresponds to a distance of 210 $(100/H_0)$ Mpc. The last two columns in Table 4 list the blue and infrared luminosities. We define the 60 μm luminosity as the energy in the band

$$L = 4\pi r^2 F_\nu \Delta\nu ,$$

where $F_\nu$ is the corrected *IRAS* flux density and $\Delta\nu$ is the bandwidth ($=3.75 \times 10^{12}$ Hz; Neugebauer *et al.* 1984). We calculate $r$ by assuming $H_0 = 100$ km s$^{-1}$ Mpc$^{-1}$ and correcting for 300 km s$^{-1}$ galactic rotation and deviation from the Hubble flow due to infall toward the Virgo Cluster of 300 km s$^{-1}$ as in Huchra and Geller (1982). Under these assumptions, the most luminous galaxy in the sample, Arp 220, could be detected above the flux limit of 2 Jy at redshifts up to 0.15.

## V. THE INFRARED LUMINOSITY FUNCTION AT 60 μm

The distribution of luminosities and the luminosity function

$$\Phi(L_i) = \frac{4\pi}{\Omega} \frac{1}{\Delta L_i} \sum_j \frac{1}{V_j}$$

are shown in Figure 3 and tabulated in Table 5. Here $\Omega/4\pi$ is the fraction of the sky covered by this survey, $\Delta L_i$ is the bin width, and $V_j$ is the volume of the universe out to which a galaxy of luminosity $L$ is observed at our flux limit. Across the top of Figure 3 we indicate the distance to which a galaxy of the corresponding luminosity can be detected at the imposed

TABLE 5

60 μm LUMINOSITY FUNCTION

| log $(L/L_\odot)$ | $\phi(L)$ (Mpc$^{-3}$ mag$^{-1}$) | $N$ |
|---|---|---|
| 8.4..... | $4.7 \times 10^{-3}$ | 1 |
| 8.8..... | $1.2 \times 10^{-2}$ | 8 |
| 9.2..... | $4.9 \times 10^{-3}$ | 8 |
| 9.6..... | $9.5 \times 10^{-4}$ | 7 |
| 10.0..... | $6.9 \times 10^{-4}$ | 20 |
| 10.4..... | $1.7 \times 10^{-4}$ | 15 |
| 10.8..... | $2.5 \times 10^{-5}$ | 7 |
| 11.2..... | $3.0 \times 10^{-6}$ | 4 |
| 11.6..... | $4.9 \times 10^{-7}$ | 2 |

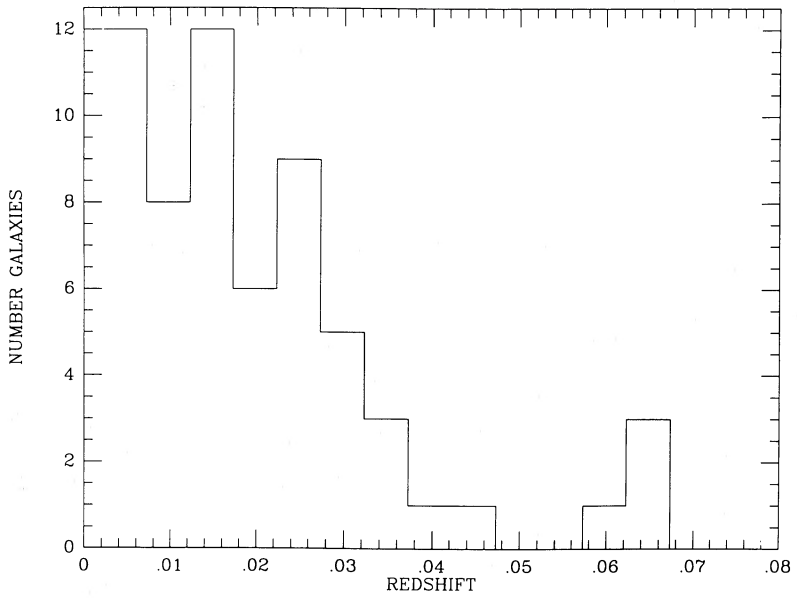


FIG. 2.—The redshift distribution of galaxies in the sample

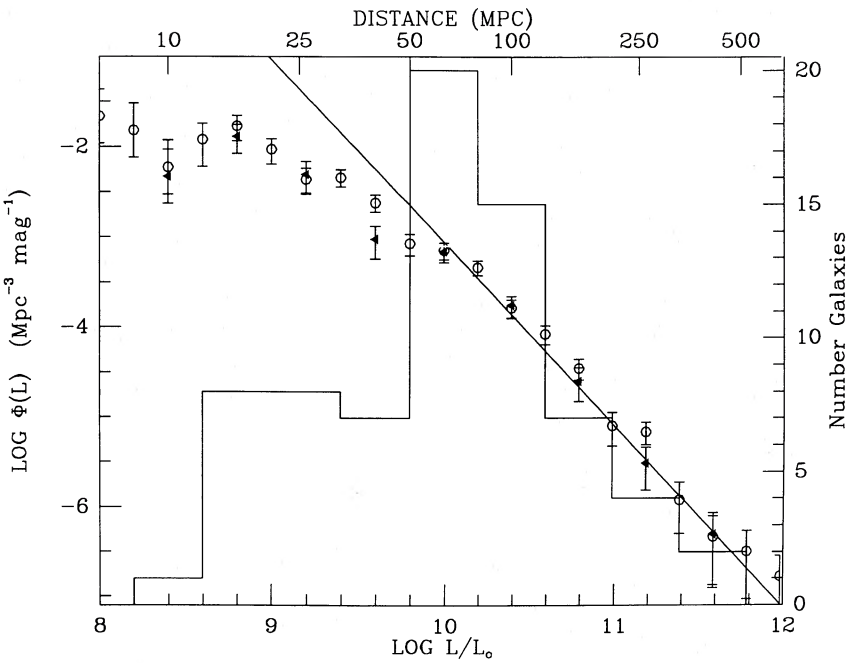


FIG. 3.—The 60 $\mu$m luminosity function. The filled triangles are from this survey; the open circles are from the complete sample [$F(60) > 0.85$ Jy] studied by Lawrence *et al.* (1986). The error bars are proportional to $N^{1/2}$. The histogram is the number count in each bin (*right axis*). The line shows a best-fit power law for $L > 10^{10}\ L_\odot$. The top margin gives the distance to which a galaxy of the corresponding luminosity could be detected at $F(60) > 2$ Jy.

limit of 2 Jy. Uncertainties in the luminosity function were calculated assuming Poisson distribution errors, proportional to $N^{1/2}$; we have ignored errors in the luminosities due to uncertainties in the infrared fluxes and deviations from Hubble flow which are not completely eliminated by our corrections for Virgocentric motion. The derived luminosities range from $4 \times 10^8\ L_\odot$ for NGC 4062 to $5 \times 10^{11}\ L_\odot$ for Arp 220.

To describe these data in a useful analytical form, we have tried both a Schechter (1976) function and a single power law. Neither yielded a good fit; at high luminosities the density lies above that expected for a Schechter function, and at low luminosities the density is less than expected for a single power law. The solid line shown in Figure 3 is a best-fit power law to our data above $10^{10}\ L_\odot$ of $\phi(L) = 1.4 \times 10^{17}(L/L_\odot)^{-2}$ Mpc$^{-3}$ mag$^{-1}$. The slope is confined to a range of $-1.5$ to $-2.2$ with 68% confidence, and the reduced $\chi^2$ is 0.60.

These results are in substantial agreement with other derivations of the luminosity function of infrared-bright galaxies. Soifer *et al.* (1986) studied a complete sample of 217 galaxies brighter than 5 Jy at 60 $\mu$m and also derived a slope of $-2.0$ for $L > 10^{10}\ L_\odot$. Lawrence *et al.* (1986) analyzed a somewhat larger sample of galaxies comprising several different flux limits. Using their total sample, they deduced that the infrared luminosity function has a slope of $-2.5$ at the highest luminosities. However, for the subset of their data which is complete above 0.85 Jy, we find good agreement with our results (Fig. 3). Vader and Simon (1986) studied a complete sample of 68 galaxies with $F(60) > 0.5$ Jy and also derived a luminosity function consistent with ours. A large, but less well-defined sample was studied by Rieke and Lebofsky (1986); they also found that the distribution of total infrared luminosity could be described by a law of the form $\phi(L_{IR}) \sim {L_{IR}}^{-2}$ at high luminosities.

## VI. INTRINSIC PROPERTIES OF THE SAMPLE

### *a) Infrared Colors*

To test whether the predominant infrared emission mechanism changes as a function of luminosity within our sample, we searched for luminosity-dependent parameters. Figure 4 compares the infrared colors with the 60 $\mu$m luminosity. The best linear fits (ignoring upper limits) to these data are

$$\log \frac{F_{12}}{F_{60}} = -0.20 \pm 0.04 \log L_{60} + 0.8 \pm 0.4\ , \quad r = -0.5$$

$$\log \frac{F_{25}}{F_{60}} = 0.00 \pm 0.04 \log L_{60} - 0.9 \pm 0.4\ , \quad r = -0.01$$

$$\log \frac{F_{60}}{F_{100}} = 0.10 \pm 0.02 \log L_{60} - 1.3 \pm 0.2\ , \quad r = 0.5\ .$$

Thus there appears to be a marginally significant correlation between the 60 $\mu$m to 100 $\mu$m flux ratio and 60 $\mu$m luminosity, and a marginally significant anticorrelation between the 12 $\mu$m to 60 $\mu$m flux ratio and 60 $\mu$m luminosity. In contrast, the 25 $\mu$m to 60 $\mu$m flux ratio appears to be completely uncorrelated with 60 $\mu$m luminosity.

A correlation between 60 $\mu$m to 100 $\mu$m flux ratio and 60 $\mu$m luminosity has been reported previously, in studies of other samples of galaxies (Miley, Neugebauer, and Soifer 1985). An interpretation of this phenomenon is suggested by the observation that a number of the most luminous galaxies are remarkably compact infrared sources (Becklin 1986; Low 1986). Thus if dust in galaxies is concentrated in two components, consisting of warm clouds near the nucleus and cooler clouds associated with the disk, the observed color-luminosity correlation

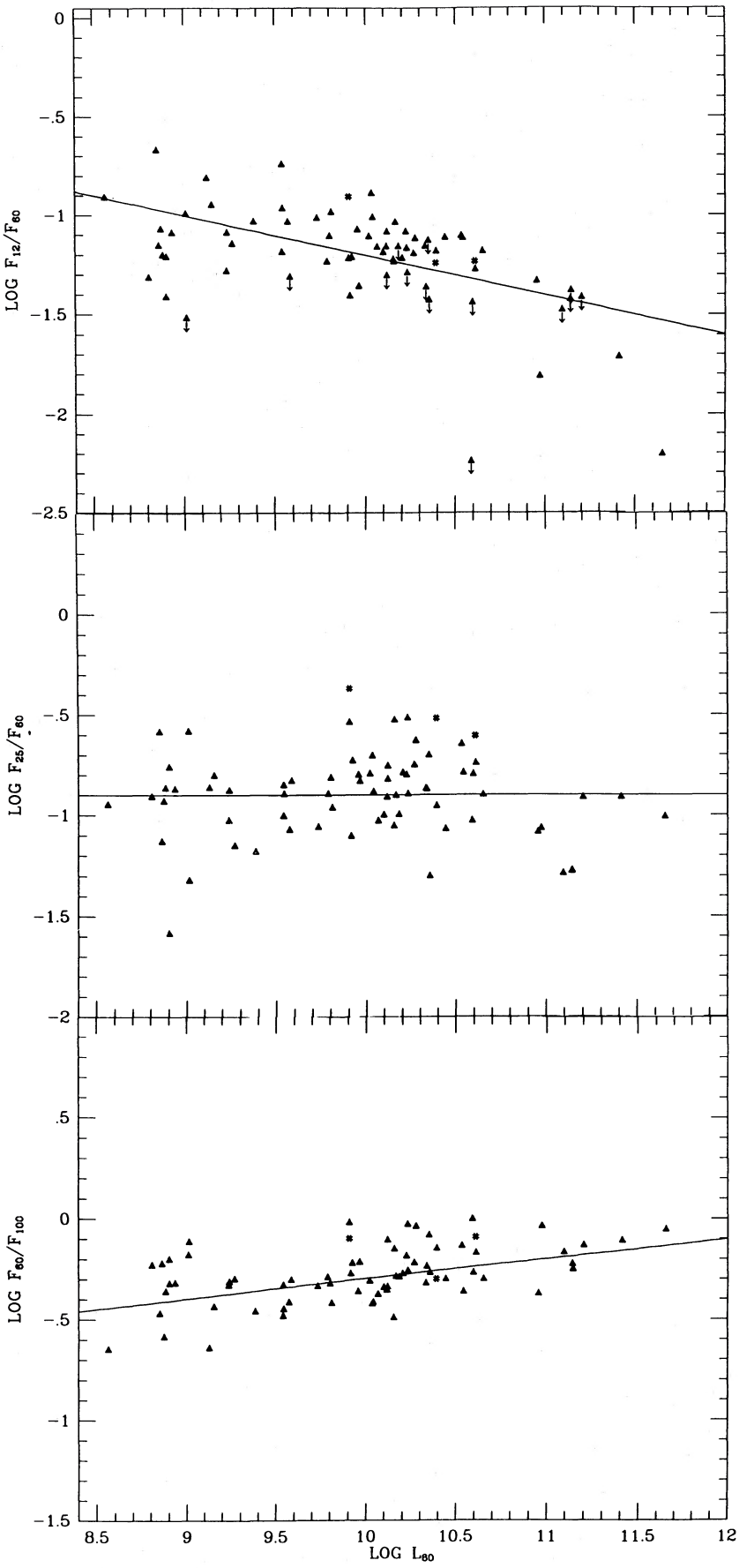


FIG. 4.—Infrared colors vs. 60 $\mu$m luminosity. The solid lines give the best linear fits to the data, excluding upper limits. The Seyfert galaxies are indicated by asterisks.

may be attributed to an increase in the luminosity of the nuclear component.

The anticorrelation of $F(12)/F(60)$ and 60 $\mu$m luminosity may be due to systematic variations in spectral features within the 12 $\mu$m band as a function of luminosity. Spectra of the highest luminosity galaxy in our sample, Arp 220, show that its 12 $\mu$m continuum is depressed by strong ($\tau[10\ \mu m] \sim 2$) silicate absorption (Rieke *et al.* 1985). The observed correlation might result from less obscuration in the less infrared-luminous galaxies. Alternatively the correlation might be produced by an increasing role of dust emission features within the 12 $\mu$m bandpass in galaxies of lower infrared luminosity. We point out that there is a single galaxy, PSC 13126+2452, with an anomalously low 12 $\mu$m flux density; its colors at longer wavelengths are normal for its luminosity and its optical spectrum is typical of the galaxies in this sample.

### b) *Distribution of Blue Luminosities*

Figure 5 shows the absolute magnitude distribution of our IR-selected sample, the Center for Astrophysics (CfA) blue-selected sample from Huchra *et al.* (1983), and the CfA spirals. This figure clearly shows that the galaxies in our sample have a narrower range of absolute blue magnitude than those of an optically selected sample. The mean for this sample is $-19.2$ with a standard deviation of only 0.8. We find that *IRAS* undersamples galaxies of low absolute blue luminosity. There also appears to be a deficiency of galaxies of high blue luminosity. A Kolmogorov-Smirnov test gives a 95% probability that the two samples are not derived from the same parent population.

We also see a difference in the blue magnitude distributions of *IRAS* galaxies and CfA spirals. A Kolmogorov-Smirnov test gives a 99% probability that the *IRAS* galaxies are not drawn from the same parent population as the CfA spiral galaxies. However, a Mann-Whitney test shows that there is only a 1 $\sigma$ difference in the medians. Thus, we conclude that the distributions are different in that the *IRAS* sample excludes galaxies of low and very high blue luminosity, and as a result, has a narrower range in blue luminosity. Because of this, the infrared excess $L(60)/L(B)$ is closely correlated (correlation coefficient = 0.89) with absolute infrared luminosity (Fig. 6). The solid line shows the position of a galaxy of $M_B = -19.2$; the dashed lines indicate the dispersion in $M_B$.

### c) *Spectral Properties*

For a rough estimate of nuclear activity in these galaxies, we use a method similar to that outlined by Baldwin, Phillips, and Terlevich (1981) to classify the emission-line spectra of extragalactic objects. Galaxies are segregated by type in the [O III]/H$\beta$ vs. [N II]/H$\alpha$ plane; Seyfert galaxies fall in the range $\log([O\ III]/H\beta) > 0.2$, $\log([N\ II]/H\alpha) > -0.3$. Galaxies with $\log([N\ II]/H\alpha) < -0.3$ are generally classified as H II region galaxies. An advantage to using these ratios is that they are relatively insensitive to reddening; a disadvantage is that a galaxy's position on this plot is a function of its metallicity.

We classify NGC 4922B and UGC 7064A as Seyfert 2 galaxies. NGC 4253 is classified as Seyfert 1 as $\log([O\ III]/H\alpha) > 0.3$ and broad permitted lines are observed. Nine galaxies are classified as H II region galaxies (see Figs. 7, 8, and 9). This method of classifying galaxy spectra has many uncertainties (see Baldwin, Phillips, and Terlevich 1981), but it does give an estimate of the percentage of active galaxies in an IR-selected sample. We find 4%, which is not significantly different from the 2.3% found by Huchra and Burg (1986) for a blue-selected sample, given the small size of our sample and the

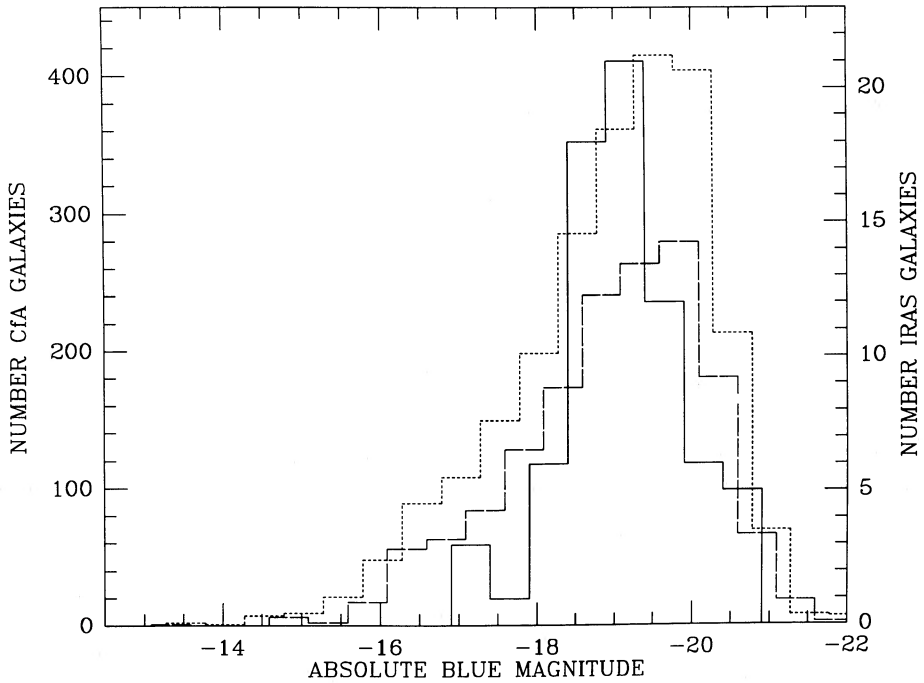


FIG. 5.—The distribution of absolute blue magnitudes of the *IRAS* sample (*solid histogram*), the CfA sample (*dotted histogram*), and the CfA spirals (*dashed histogram*).

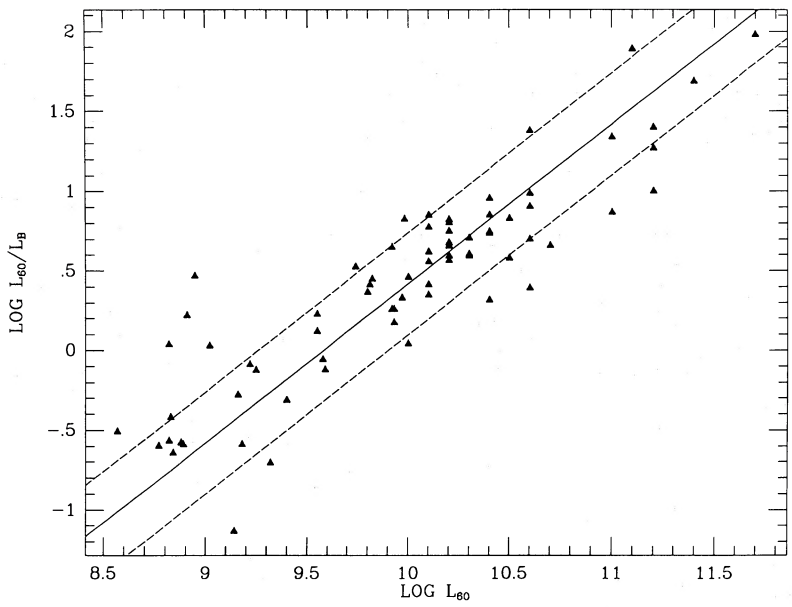


FIG. 6.—Infrared excess $L(60)/L_B$ vs. 60 $\mu$m luminosity. The solid line shows the position of a galaxy of $M_B = -19.2$; the dashed lines indicate the dispersion in $M_B$.

uncertainties in the classification scheme. Thus there is not a large overabundance of active galactic nuclei (AGNs) in this IR-bright sample.

The Seyfert galaxies do not have extraordinarily high 60 $\mu$m luminosities; they range from $8 \times 10^9$ $L_\odot$ to $4 \times 10^{10}$ $L_\odot$. Their nuclear activity, as measured by the ratio of equivalent widths, [O III]/H$\beta$ (Baldwin, Phillips, and Terlevich 1981), lies in the same range as the non-Seyfert galaxies in our sample (Fig. 10). Thus unobscured nuclear activity is probably not a strong contributor to the 60 $\mu$m flux in the galaxies in our sample.

We note that the infrared spectral energy distributions of the active galaxies in our sample are distinctive in that their $F(25)/F(60)$ ratios are all higher than other galaxies of the same 60 $\mu$m luminosities (see Fig. 4). The relatively high 25 $\mu$m fluxes of active galaxies has been noted by Miley, Neugebauer, and Soifer (1985).

### *d) Morphology*

Morphological classifications could be estimated from the POSS plates for about 85% of the galaxies in our sample. Types are plotted in Figure 11 as a function of luminosity. No correlation is apparent. However, the galaxies in our sample which lack morphological classifications are among the most luminous observed, and a correlation between shape and luminosity might not be apparent within the limited range of luminosities of the subsample for which morphological types are available. Note that few galaxies in our sample have types

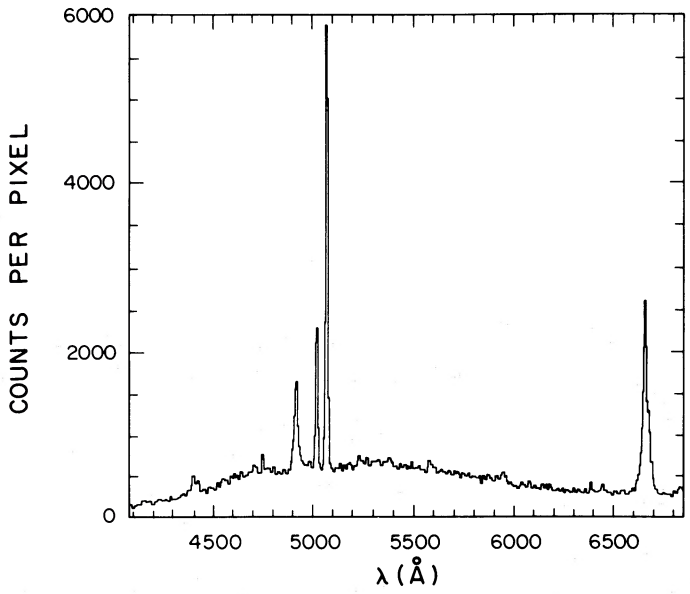


FIG. 7.—Spectrum of NGC 4253, classified as Seyfert 1

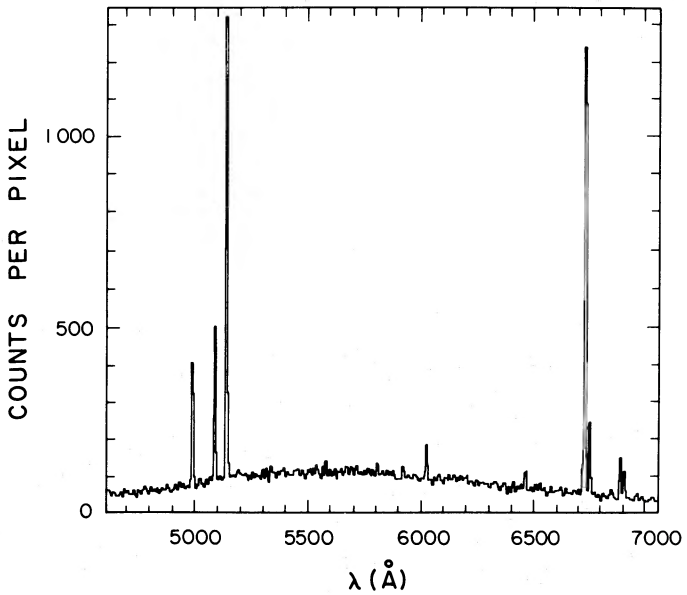


FIG. 8.—Spectrum of MK 727, classified as an H II region galaxy

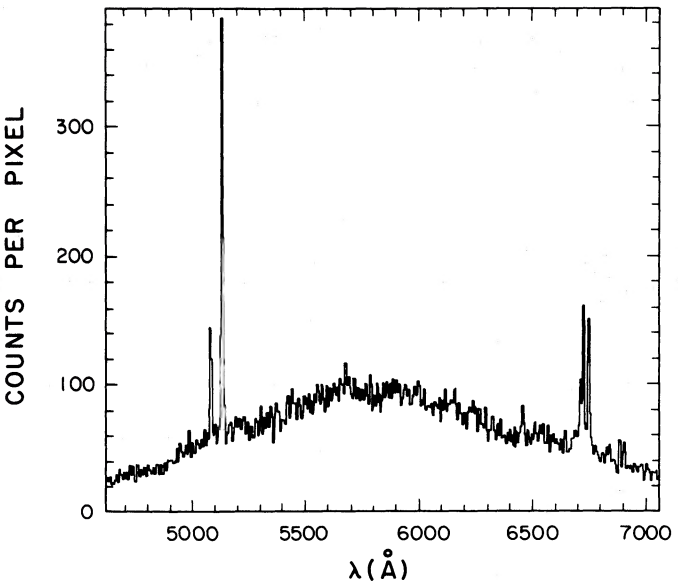


FIG. 9.—Spectrum of UGC 7064a, classified as Seyfert 2

earlier than S0 (type < 0); this is in agreement with the results of Wolstencroft *et al.* (1985).

However, there may be some correlation of infrared luminosity with the presence of a perturbing neighbor. At least half of the galaxies in our sample having $L(60) > 10^{11}\ L_{\odot}$ are found in multiple systems, and we find that 18% ± 5% of all of the galaxies in our sample are classified as peculiar or are in pairs (see Table 3). This value is significantly higher than the fraction (6.4% ± 0.1%) of peculiar or paired galaxies found in an optically selected sample (Arp and Madore 1977). Lonsdale, Persson, Matthews (1984) found that an even larger fraction (37%) of the bright galaxies in the *IRAS* mini-survey were in interacting groups. If emission from dust heated by recent star formation is a major contributor to the far-infrared flux, these results are consistent with the suggestion by Larson and Tinsley (1978) that interactions between galaxies can trigger star-formation bursts.

### *e) Space Distribution*

Comparing the space distribution of our sample with that of an optically selected sample, we find that the *IRAS* galaxies trace the cellular pattern of galaxies observed by de Lapperent, Geller, and Huchra (1986); however, a density enhancement in the core of Coma the size of the optical density enhancement is not observed. Defining the boundaries of Coma by $12^{h}30^{m} < \alpha < 13^{h}30^{m}$, $26\overset{\circ}{.}5 < \delta < 32\overset{\circ}{.}5$, 5000 km $s^{-1} < v < 9000$ km $s^{-1}$, we find that the IR density/$B$ density ratio in Coma is $\frac{1}{3}$ that of the mean of the remainder of our box. This is consistent with the morphology of infrared-bright galaxies, in that spirals are the most common type in our sample and in other samples of *IRAS* galaxies (Wolstencroft *et al.* 1985), while Coma is dominated by Es and S0s (Dressler 1980). If the mass in the universe is concentrated in clusters, and if $M/L_{\rm BLUE}$ is equal among spirals and ellipticals (or if $M/L_{\rm BLUE}$ is greater for S0s and Es), then *IRAS* does not trace the mass density. This introduces errors into the gravitational dipole moment derived by Yahil, Walker, and Rowan-Robinson (1985) and Meiksen and Davis (1986).

## VII. DISCUSSION

An analysis of the colors and morphology of the galaxies in our sample suggests that galaxies exceeding $L(60) = 10^{11}\ L_{\odot}$ differ significantly from those having $L(60) < 10^{9}\ L_{\odot}$. The eight high-luminosity galaxies have

$$F(12)/F(60) < 0.047\ ,$$

$$0.42 < F(60)/F(100) < 0.92\ ,$$

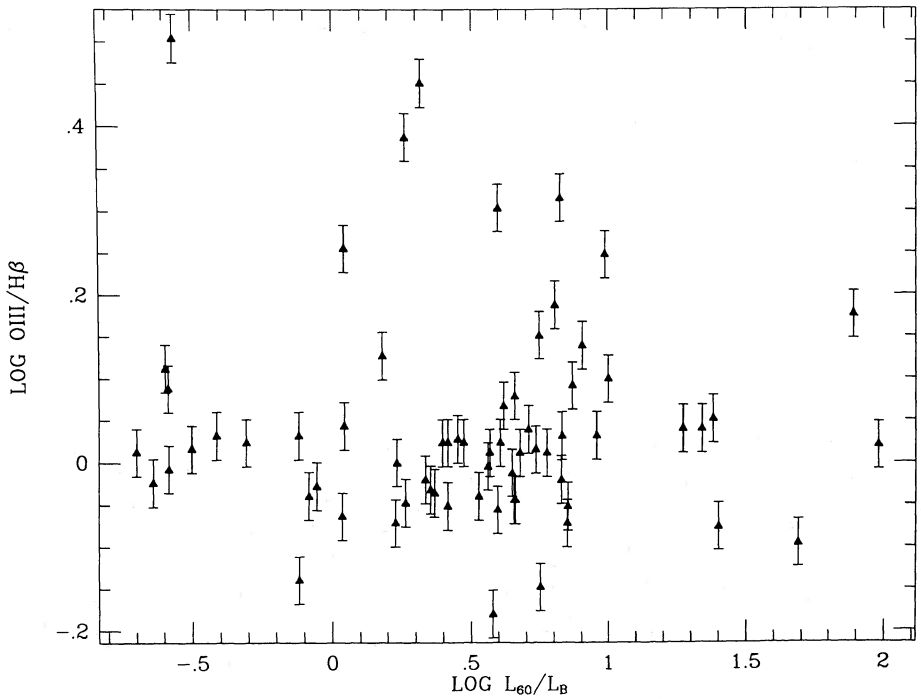


FIG. 10.—Nuclear activity index O III/H$\beta$ vs. IR excess

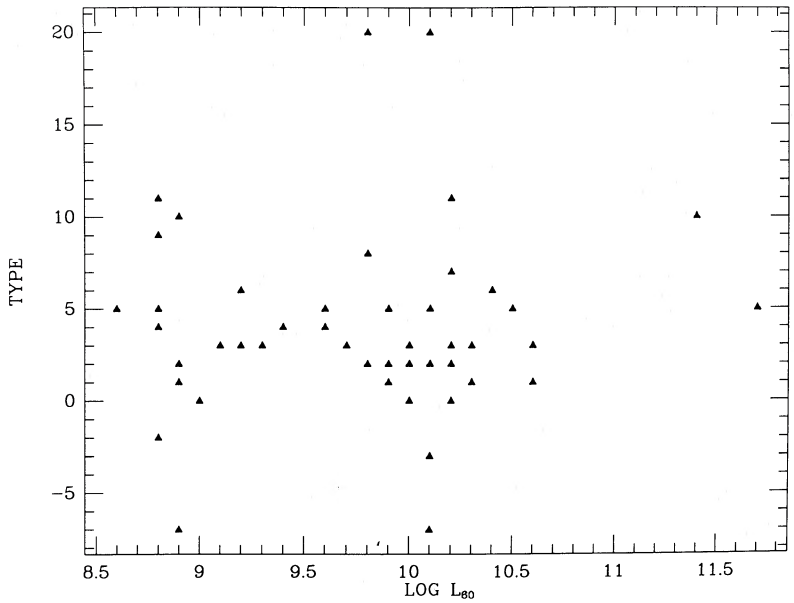


FIG. 11.—Morphological type vs. 60 $\mu$m luminosity. The scale used is that defined by de Vaucouleurs *et al.* (1976), and the types were taken from this paper and Huchra *et al.* (1983).

while the nine low-luminosity galaxies have

$$0.045 < F(12)/F(60) < 0.20 ,$$

$$0.23 < F(60)/F(100) < 0.63 .$$

A $t$-test shows that these distributions differ from one another at the 98% confidence level. At least half of the high-luminosity galaxies are in multiple systems, while all of the low-luminosity galaxies are isolated. These facts suggest that the derived infrared luminosity function is a superposition of two distributions; one, associated with normal spirals, may approximate a Schechter function and dominate at low luminosities. The other, associated with interacting systems, dominates at high luminosities, and does not appear to follow a Schechter function in that no exponential cutoff is observed at its high-luminosity extreme.

The Schechter luminosity function was derived (Press and Schechter 1974) by an argument involving the mass spectrum of primordial fluctuations in the early universe and assumes a constant light-to-mass ratio for galaxies. The excess density of luminous infrared galaxies above that expected for a Schechter function may reflect a higher light-to-mass ratio in the most luminous infrared galaxies. This suggestion is consistent with the hypothesis that the efficiency of massive star formation is highest among the most luminous infrared galaxies (Young *et al.* 1986).

The lack of galaxies of low blue luminosity in our sample may be due to differences in the proximity of the dust to the heating sources in galaxies of different blue luminosity. It seems plausible, for example, that galaxies of high blue luminosity may have undergone a recent burst of star formation, and have a higher fraction of their mass concentrated in H II regions still associated with molecular clouds.

## VIII. CONCLUSIONS

In agreement with previous studies of the luminosity function of infrared-bright galaxies, we find that (1) a simple power law of the form $-2.0 \pm 0.5$; 0.2 is a good fit to the distribution for luminosities from $10^{10}$ to $10^{12}$ $L_{\odot}$, (2) there is no indication of an exponential dropoff in the luminosity function at high energies, and (3) there is a flattening of the luminosity function at $L < 10^{10}$ $L_{\odot}$.

A review of the infrared colors and morphology of the galaxies in this sample show that two different populations may contribute to the observed luminosity function. The highest luminosity galaxies are typically found in multiple, possibly interacting, systems and exhibit marginally narrower infrared spectral energy distributions than the isolated spirals which predominate at low luminosities. Further morphological studies of a complete sample of galaxies detected by *IRAS* are needed to determine how the luminosity function of interacting galaxies differs from that of noninteracting galaxies.

Comparison of the properties of galaxies included in the sample studied here and an optically selected sample show that infrared-bright galaxies come from a different population than the majority of optically bright galaxies. In particular, galaxies of low blue luminosity are not strong infrared emitters. There is also a difference in the spatial distribution of IR-selected and optical-selected galaxies, in the sense that the density enhancement seen in optical surveys of rich clusters is not observed at the same level in the infrared. This difference is probably related to the poor representation of ellipticals in the infrared survey and suggests that *IRAS* is systematically underestimating the mass in rich clusters. This effect may introduce significant errors into a gravitational dipole moment derived on the assumption that the distribution of infrared-bright galaxies is simply related to the mass distribution of the universe.

We would like to thank J. Peters, E. Horine, and S. Tokarz for help in obtaining and reducing the data, and E. Feigelson and N. Z. Scoville for helpful comments. This work was partially supported by the Smithsonian Institution, by AFOSR grant no. 85-0057, by the NASA *IRAS* Extended Mission at IPAC, and by the general investigator program at IPAC.

## APPENDIX

Both *K*-corrections and color corrections must be made to the *IRAS* flux densities in order to determine the flux densities in the rest frame of each source at constant effective wavelengths. The corrections applied in this paper were determined in a four-step process.

1. We computed the *total* flux in each of the four *IRAS* bands by integrating the energy distribution that was assumed in the derivations of the *IRAS* flux densities, ($S \sim \lambda^{-1}$),

$$F_i = S_i \lambda_i \int_0^\infty \frac{R(\lambda)}{\lambda} d\lambda ,$$

where $S_i$ is the uncorrected flux density and $R(\lambda)$ is the spectral response function.

2. We then made a look-up table of the total flux expected for blackbody sources of various temperatures ($T$) and redshifts ($z$):

$$H_i = \int_0^\infty \frac{B[\lambda/(1+z), T]}{(1+z)} R(\lambda) d\lambda ,$$

where $B$ = the Planck function.

3. By comparing the ratios of integrated flux densities for a source at a known redshift with the look-up table, we deduce three color temperatures, $T_1$, $T_2$, $T_3$, corresponding to $F(12)/F(25)$, $F(25)/F(60)$, and $F(60)/F(100)$.

4. The flux densities in the rest frames of the sources are then evaluated on the assumption that the spectral energy distributions in adjacent bands match those of a blackbody,

$$S_i = \frac{B(\lambda_i, T_i) F_i}{H_i} ,$$

where $S_i$ is the flux density at the effective wavelength of band $i$ in the rest frame of the source, and the temperatures $T_i$ are $T_1$ for $\lambda = 12$ $\mu$m, $(T_1 + T_2)/2$ for $\lambda = 25$ $\mu$m, $(T_2 + T_3)/2$ for $\lambda = 60$ $\mu$m, and $T_3$ for $\lambda = 100$ $\mu$m.

*Note added in proof.*—In an effort to understand the completeness of the present sample, we have obtained additional photometry, using the Add-Scan program at IPAC, of all 14 galaxies in the UGC which are in the region of the sky studied in this paper and are listed in the PSC with 60 $\mu$m flux densities between 1.5 and 2.0 Jy. With this more accurate photometry, we found that one object, UGC 10273 (=PSC 16107+2824), had a flux density at 60 $\mu$m exceeding the lower limit of our sample. The heliocentric velocity of this object is 7381 $\pm$ 38 km s$^{-1}$. Its corrected flux densities are 0.14 (0.17), 0.24 (0.04), 2.30 (0.095), and 5.21 (0.02) Jy, at effective wavelengths of 12, 25, 60, and 100 $\mu$m, where the numbers in parentheses are the percentage by which the *IRAS* photometry was corrected for the bandwidth of the filters and the redshift. The luminosity of this galaxy in the 60 $\mu$m band is 10.2 dex, near the median of our sample. This galaxy is classified as Sd (i.e., morphological class 7) and has $m(B) = 15.3$ mag, so that its optical luminosity is also near the median of our sample.

We have recently received a preprint from Soifer *et al.*, describing an extended study of the luminosity function and other properties of the brightest galaxies detected by *IRAS*. These authors also find that galaxies selected on the basis of their infrared brightness exhibit a narrow range in blue luminosities.

## REFERENCES


Arp, H. C., and Madore, B. F. 1977, *Quart. J.R.A.S.*, **18**, 234.
Baldwin, J. A., Phillips, M. M., and Terlevich, R. 1981, *Pub. A.S.P.*, **93**, 5.
Becklin, E. E. 1986, in *Proc. Star Formation in Galaxies Conference* (Pasadena: California Institute of Technology), in press.
de Lapparent, V., Geller, M. J., and Huchra, J. P. 1986, *Ap. J. (Letters)*, **302**, L1.
de Vaucouleurs, G., de Vaucouleurs, A., and Corwin, H. R. 1976, *Second Reference Catalog of Bright Galaxies* (Austin: University of Texas).
Dressler, A. 1980, *Ap. J. Suppl.*, **42**, 656.
Gioia, I. M., *et al.* 1984, *Ap. J.*, **283**, 495.
Huchra, J. P. 1976, *A.J.*, **81**, 952.
Huchra, J. P., and Burg, T. 1986, in preparation.
Huchra, J. P., Davis, M., Latham, D., and Tonry, J. 1983, *Ap. J. Suppl.*, **52**, 89.
Huchra, J. P., and Geller, M. J. 1982, *Ap. J.*, **257**, 423.
*IRAS Point Source Catalog.* 1985, Joint *IRAS* Science Working Group (Washington D.C.: US Government Printing Office) (PSC).
*IRAS Small Scale Structures Catalog.* 1986, prepared by G. Helou and D. Walker (Washington D.C.: US Government Printing Office) (SSS).
Larson, R. B., and Tinsley, B. M. 1978, *Ap. J.*, **219**, 46.
Latham, D. 1982, in *IAU Colloquium 67, Instrumentation for Astronomy with Large Optical Telescopes*, ed. C. M. Humphries (Dordrecht: Reidel), p. 259.
Lawrence, A., Walker, D., Rowan-Robinson, M., Leech, K. J., and Penston, M. V. 1986, *M.N.R.A.S.*, **219**, 687.
Lonsdale, C. J., Persson, S. E., and Matthews, K. 1984, *Ap. J.*, **287**, 95.
Low, F. J. 1986, in *Proc. Star Formation in Galaxies Conference* (Pasadena: California Institute of Technology), in press.
Low, F. J., *et al.* 1984, *Ap. J. (Letters)*, **278**, L19.
Meiksin, A., and Davis, M. 1986, *A.J.*, **91**, 191.
Miley, G. K., Neugebauer, G., and Soifer, B. T. 1985, *Ap. J. (Letters)*, **293**, L11.
Neugebauer, G., *et al.* 1984, *Ap. J. (Letters)*, **278**, L1.
Nilson, P. 1973, *Uppsala General Catalog of Galaxies* (*Uppsala Astr. Obs. Ann.*, Vol. **6**).
Press, W. H., and Schechter, P. 1974, *Ap. J.*, **187**, 425.
Rice, W., Persson, C. J., Soifer, B. T., Neugebauer, G., and Kopan, E. 1986, in preparation.
Rieke, G. H., *et al.* 1985, *Ap. J.*, **290**, 116.
Rieke, G. H., and Lebofsky, M. J. 1986, *Ap. J.*, **304**, 326.
Rowan-Robinson, M., *et al.* 1984, *Ap. J. (Letters)*, **278**, L7.
Schechter, P. 1976, *Ap. J.*, **203**, 297.
Soifer, B. T., *et al.* 1986, *Ap. J. (Letters)*, **303**, L41.
Vader, J. P., and Simon, M. 1986, in *Proc. Star Formation in Galaxies Conference* (Pasadena: California Institute of Technology), in press.
Wolstencroft, R. D., Clowes, R. G., Kalafi, M., Leggett, S. K., MacGillivray, H. T., and Savage, A. 1986, in *Proc. Light on Dark Matter Conference*, in press.
Yahil, A., Walker, D., and Rowan-Robinson, M. 1985, *Ap. J. (Letters)*, **301**, L1.
Young, J. S., Schloerb, F. P., Kenney, J. D., and Lord, S. D. 1986, *Ap. J.*, **304**, 443.
Zwicky, R., Karpowicz, M., Kowal, C., Herzog, E., and Wild, P. 1961–1966, *Catalog of Galaxies and of Clusters of Galaxies* (Pasadena: California Institute of Technology), Vols. **1–6**.



J. P. HUCHRA: Center for Astrophysics, 60 Garden Street, Cambridge, MA 02138

S. G. KLEINMANN: Department of Physics and Astronomy, University of Massachusetts, Amherst, MA 01003

F. J. LOW: Steward Observatory, University of Arizona, Tucson, AZ 85721

B. J. SMITH: Five College Astronomy Department, University of Massachusetts, Amherst, MA 01003